PAPER • OPEN ACCESS

Wind Farm Wakes and Farm-to-Farm Interactions: Lidar and Wind Tunnel Tests

To cite this article: W.U. Ahmed *et al* 2024 *J. Phys.: Conf. Ser.* **2767** 092105

View the article online for updates and enhancements.

Wind Farm Wakes and Farm-to-Farm Interactions: Lidar and Wind Tunnel Tests

W.U. Ahmed[1], C. Moss[1], S. Roy[1], M. Shams Solari[1], M. Puccioni[1,2], K. Panthi[1], P. Moriarty[3], G.V. Iungo[1]

[1] Center for Wind Energy, Wind Fluids and Experiments (WindFluX) Laboratory, Mechanical Engineering Department, The University of Texas at Dallas, 800 W. Campbell Rd., Richardson, TX 75080, U.S.A.

[2] Lawrence Livermore National Laboratory, 7000 East Ave., Livermore, CA 94550, U.S.A.

[3] National Renewable Energy Laboratory, 15013 Denver W. Pkwy., Golden, CO 80401, U.S.A.

E-mail: `valerio.iungo@utdallas.edu`

Abstract. Recent experimental and numerical evidence has shown that the cumulative wake generated from the overlapping of multiple wakes within a wind farm could reduce power performance and enhance fatigue loads of wind turbines installed in neighboring downstream wind farms and may also extend up to distances one order of magnitude larger than those typically considered for intra-farm wake interactions. Similar to individual wind turbine wakes, wind farm wakes have a velocity deficit and added turbulence intensity, both affected by the turbine rotor thrust forces and the incoming turbulence intensity. Therefore, the evolution of wind farm wakes will vary for different operational and atmospheric conditions. In this paper, lidar measurements collected during the American WAKE experimeNt (AWAKEN) and wind tunnel tests of wind farms reproduced by porous disks are leveraged to investigate wind farm wakes.

Keywords: Wind farm, wake, farm-to-farm interactions, lidar, wind tunnel

1. Introduction

With the increasing demand for wind energy, wind farms are being built closer together that, in turn, may lead to mutual interactions similar to those occurring among neighboring wind turbines. Wakes generated by an upstream wind farm can affect wind conditions experienced by a downwind turbine array, leading to reduced wind speed and power capture along with enhanced turbulence intensity and added fatigue loads. Individual wind turbine wakes evolve and merge to form wind farm wakes, wherein downwind dynamics are affected by atmospheric stability [1, 2].

Measurements of offshore wind farm wakes have shown downwind extents of a few tens of kilometers under stable atmospheric conditions [1, 3], thus corroborating the risks on wind resources for neighboring wind turbine arrays. Wind farm wakes have been studied with instruments that cover large measurement areas, such as satellite

synthetic aperture radar (SAR) [4, 5], dual Doppler radar (DR) [6], measurements from research aircraft [1], and lidar [3, 7]. These measurement techniques have demonstrated that wind farm wakes can persist for very long distances. A wind speed deficit of 2% is observed 5-20 km downstream of wind farms compared to the unobstructed flow upstream [4]. Studies also found that the wind farm wakes persist at least 7.7 km [5], 17 km [6], and 55 km under stable and weakly unstable stratification [3]. These studies identified a region of undisturbed flow at the side of the wake profiles to evaluate the presence of the wake. The wake length is estimated based on a wind speed deficit of at least 0.1 m/s compared to the undisturbed flow (at the side of the wake profiles) [1]. These authors observed that under stable stratification, the wake length can reach up to 70 km downstream of a wind farm. Furthermore, findings from large-eddy simulations (LES) indicated that wakes generated from very large wind farms characterized by smaller turbine spacing and operating within shallow stable boundary layers can extend beyond 100 km [8]. Further, denser wind farms are characterized by enhanced wake extent in the downstream direction and near-wake velocity deficit [2].

Farm-to-farm interactions have been detected in terms of reduced power capture and increased turbulence intensity, TI, by leveraging supervisory control and data acquisition (SCADA) data [9, 10]. For a wind farm located 15 km downstream of another wind farm; a reduction in power of 30% of the expected power was observed [9]. By combining SCADA data [11] and LES [12], it was suggested that wind farm wakes predominantly affect the power production of the first row of a downstream farm.

In this paper, we leverage measurements performed with scanning Doppler lidars performed for the American WAKE experimeNt (AWAKEN) experiment to investigate physical processes associated with the generation and evolution of wind farm wakes. These measurements were collected at a location between two large wind farms. For a more accurate and idealized investigation of wind farm wakes, experiments were also performed at the University of Texas at Dallas (UTD) Boundary Layer and Subsonic Tunnel (BLAST) by modeling wind farms as arrays of porous disks with different thrust coefficients and installed in different layouts (i.e. streamwise and spanwise spacing). The overarching goal of this project is to provide guidelines for developing improved models for wind farm wakes and their mutual interactions.

2. Lidar experimental methodology

One of the main objectives of the AWAKEN experiment is to generate comprehensive observations of the interactions between the atmospheric boundary layer (ABL) and multiple wind farms located in the Southern Great Plains in Oklahoma. The WindFluX mobile lidar station, encompassing two scanning pulsed Doppler lidars and a surface-flux station, was deployed at the AWAKEN site C1a, which is located between two wind farms, King Plains and Armadillo Flats, having a separation distance of about 2 km along the prevailing north-south wind direction. Therefore, AWAKEN provides the opportunity to study the outflow from an upwind wind farm, the inflow for the

downwind farm, and, in turn, potential farm-to-farm interactions. Full details of the
site and the lidar deployment can be found in a recent publication [7].

The wind lidars performed different types of scans to probe flow processes governing
the downstream evolution of wakes and their merging into farm wakes. Of the two
scanning Doppler lidars installed at the site, one, a Halo Streamline XR, performed
range-height-indicator (RHI), Doppler-beam-swinging (DBS), fixed points, and plan-
position-indicator (PPI) scans. The PPI scans were directed south to study flow from the
Armadillo Flats wind farm. The other lidar, a WindCube 200S scanning unit, performed
only PPI measurements. We here focus only on the results from the 200S lidar, as it
provides better data quality over the specific region of interest. This region experiences
wind from the north, which contains trailing wakes from the King Plains wind farm,
and which we study to investigate wake merging and recovery. The Armadillo Flats
wind farm has a high likelihood of being impacted by these wakes. Thus, this condition
likely results in farm-to-farm interaction. To capture this region, the WindCube 200S
performed multiple PPI scans with elevation angles of 1°, 1.5°, 2°, 3°, and then from 4°
to 28° in steps of 2°. The PPI scans were performed between azimuth angles of 300°
to 90° with an angular resolution of 1° and an accumulation time of 0.5 s, leading to a
total time of 1380 s for all scans. A 50-m range gate was used. The scans were optimally
designed using the LiDAR Statistical Objective Analysis (LiSBOA) procedure [13]. Full
details of the scanning strategy can be found in previous work [7].

3. Lidar results

Several steps are needed to process the PPI data. First, each sampled height,
corresponding to a certain lidar range gate, is assigned a wind direction by fitting
a sinusoid function to the radial wind speed (RWS) as a function of the azimuth
angle. While the instantaneous data cannot be considered homogeneous, we aim to
study wakes, entailing that the measurements most likely will not be homogeneous.
Furthermore, while the other lidar does perform DBS scans, from which wind direction
profiles can be inferred, the measurement volume of the DBS scans suffers from the same
inhomogeneities caused by wakes. For this reason, it is difficult to accurately estimate
the wind condition, and we believe that the estimate from the PPI scans provides a
more suitable approach. This approach has been previously used with success for the
analysis of lidar data for this site [7]. No prior filtering is performed except the rejection
of RWS values with a corresponding carrier-to-noise ratio smaller than -25 dB. After
determining the wind direction at each height, the wind direction for the snapshot
is averaged over predefined 20-m-tall bins to retrieve the wind direction onto a fixed
vertical resolution. This procedure is repeated for all scans, producing a time series
of wind profiles. To provide as many height values as possible for each time stamp, a
sliding-averaging procedure is applied. A time window of 1 hour is used, centered on a
given time stamp, and wind direction profiles are averaged over this time window. If
the averaging procedure produces a standard deviation of the wind direction of 50° or

greater at a given height, that height is rejected due to high temporal variability. The result is a wind direction profile that covers as many heights as possible.

Subsequently, the horizontal wind speed, U, is estimated from the PPI scans. For each snapshot, RWS values with corresponding azimuth values greater than 45° from the wind direction interpolated to the given height from the previously determined wind direction profiles, are rejected to ensure a minimal projection of the wind velocity vector along the lidar line of sight. Under these conditions, assuming that the elevation angle, Φ, is relatively low (generally lower than 30°), given an azimuth angle Θ, and wind direction Θ_w, U can be estimated as $RWS/(\cos(\Theta - \Theta_w)/\cos\Phi)$ [7]. To estimate the unimpeded flow, the previously defined height bins are applied, with the 70th percentile in U over each height bin being taken as the free-stream U for that height, U_∞ [19]. A time-averaging procedure that is similar to the wind direction profiles is applied, with heights possessing a standard deviation greater than 40% of the mean value being rejected. Finally, U_{norm} is defined as U/U_∞.

After estimating vertical profiles of the free-stream wind direction and speed, shear and veer are determined. The shear exponent is calculated using the power law, whereas veer is defined as the slope of the best fit of wind direction against height, considering values only over the rotor heights. To understand the impact of atmospheric conditions on wind farm wakes, we apply a cluster analysis, seeking two clusters of identical wind speed, wind direction, and veer limits, but with different shear values, to highlight the impact of shear on wake behavior.

To this end, we restrict U_∞ to be between 7.5 m/s and 8.5 m/s and Θ_∞ to be between 5° and 15°, both at the turbine hub height. We do not consider limits on veer, as many cases do not have linear profiles in wind direction, leading to veer being poorly captured by a linear approximation. We define two bins, one with high shear, between 0.3 and 0.4, and one with low shear, between 0.1 and 0.2. Figure 1 plots the hub-height reconstructions on the selected PPI scans. As demonstrated in the figure, decreasing shear, which is associated with increased atmospheric instability, causes the wakes to merge more quickly, resulting in greatly reduced definition in the peaks in Figure 1(b) and (d). Further investigation is needed to determine the impact of stability on wake recovery, which may be enhanced. Other effects might also impact turbine wake merging, such as wind speed or turbine spacing. Further detailed analyses are required to tease apart these varied effects.

4. Experimental setup of the wind tunnel experiments

To complement the available field data on farm-to-farm interactions and wind farm wakes, hot-wire measurements (HWA) were performed at the boundary layer test section of the UTD BLAST wind tunnel (2.8-m width, 2.1-m height, and 30-m length). Wind farms are modeled by installing porous disks with rotor diameter, D, and hub height, h, equal to 80 mm. Considering a wind farm made of five columns, the resulting solid blockage is about 0.37%. Wind farm configurations are varied by changing the
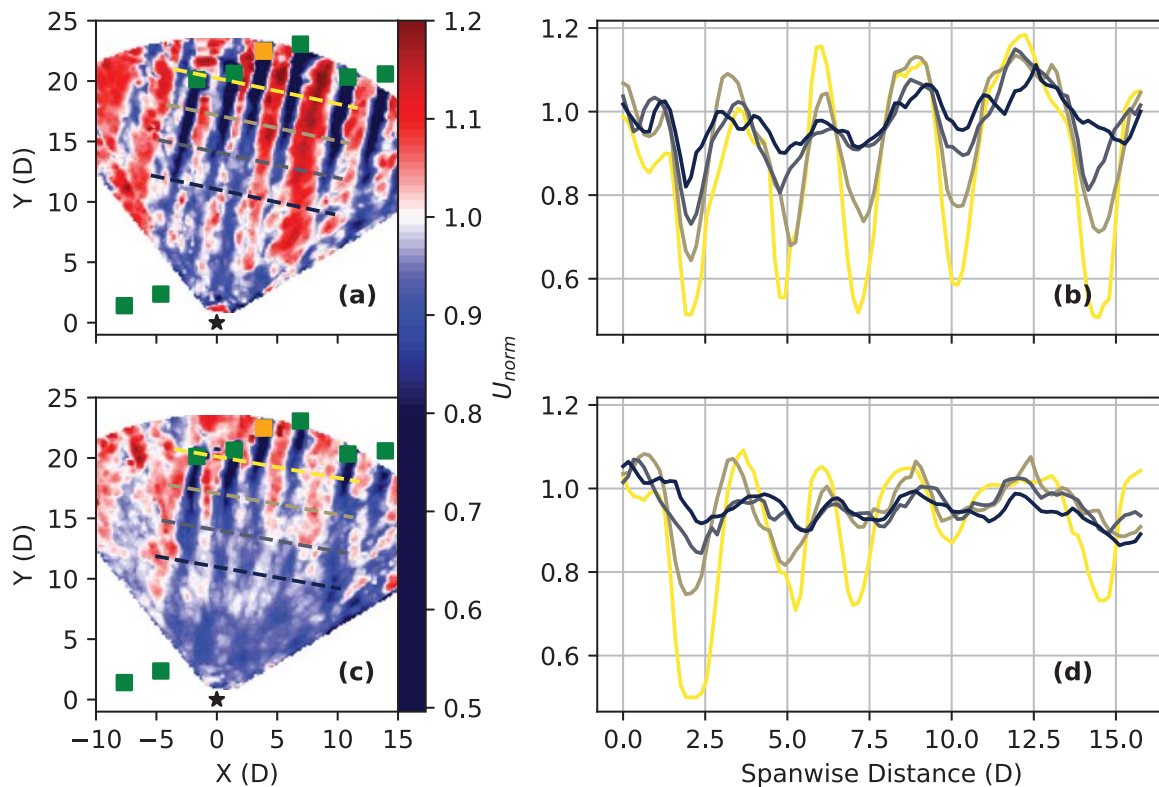
Figure 1. Hub-height reconstructions of scanning lidar data considering wind speed values between 7.5 and 8.5 m/s, wind direction values between 5° and 15°, and two shear bins, with the first keeping the shear exponent between 0.3 and 0.4 (a) and the second keeping the shear exponent between 0.1 and 0.2 (c). Transects along the streamwise direction are taken in $3D$ steps downwind from the highlighted turbine (orange square) and the velocity deficit along the transects is plotted in (b) for the high-shear bin and in (d) for the low-shear bin.

streamwise spacing, S_x (5D or 7D), spanwise spacing, S_y (3D or 2.5D), and number of turbine rows, N_r (7, 10, 13, or 15), with a fixed number of columns, $N_c = 5$. The configurations of the wind farm employed in this experiment to investigate wind farm wakes are listed in Table 4. Configurations A and B have identical S_x values of 5D, but different S_y values of 3D and 2.5D, respectively. On the other hand, configurations A and C have the same S_y value of 3D, but different S_x values of 5D and 7D, respectively. These configurations are selected to study the effect of S_x and S_y. A rendering of the wind tunnel and a configuration of a wind farm are shown in Figure 2(a) and (b), respectively. Horizontal and vertical profiles are measured at different downstream locations from the most downstream rotor disk at locations 5, 10, 15, 30, and 40D.

The design of the rotor models as porous disks is performed with decreasing outward radial solidity, thus replicating the mean profile of the streamwise velocity for the wake generated by a two-bladed wind turbine operating at the same C_t [14]. In addition, in the far wake ($X/D > 3$), the wake velocity deficit [15], the wake expansion [16], and the wake turbulence intensity [17] closely match those of wind turbines and porous disks generating similar C_t. Further, at the near wake, the double Gaussian wake

Table 1. Wind farm configurations.

Configuration (S_x, S_y)	N_c	N_r	C_t
A $(5D, 3D)$	5	7, 10, 13, 15	0.85
B $(5D, 2.5D)$	5	7, 10, 13, 15	0.85
C $(7D, 3D)$	5	7, 10	0.85
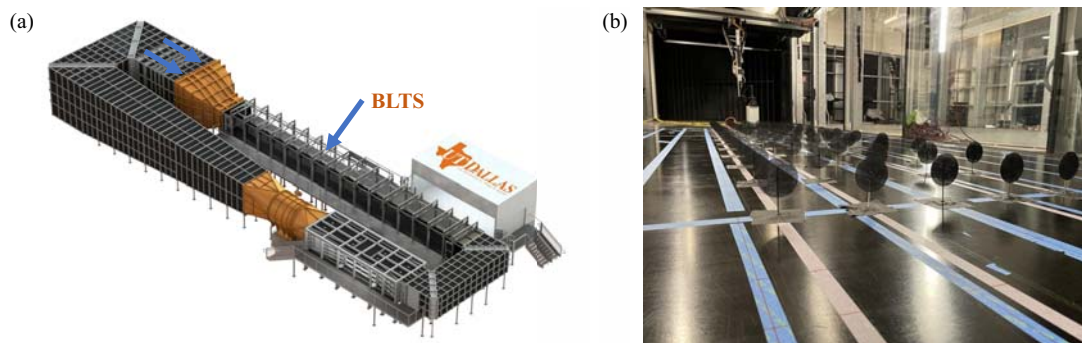
Figure 2. (a) UTD BLAST wind tunnel and (b) wind farm configuration with 15 rows, $S_x = 5D$ and $S_y = 2.5D$.

profile measured by a scanning lidar downstream of a full-scale wind turbine has been matched by varying the radial solidity of a porous disk. The wind farm configurations considered for this experiment have streamwise spacing larger than $3D$. Thus, the wakes experienced by the downstream porous disks situated at $X > 3D$ should be similar to a wake generated by a wind turbine [15].

The HWA calibration is performed inside the wind tunnel using an external calibrator manufactured by Dantec. The HWA was calibrated within the range of 1–6 m/s, and using a fourth-order polynomial function. To take into account the calibration drift in time, the methodology used in [18] is followed by measuring a reference point in between consecutive measurements.

The experiments were conducted with a free-stream velocity of approximately $U_\infty = 4.2$ m/s and $TI = 8\%$ at hub height. The boundary layer height, δ, of the turbulent boundary layer, was about 0.31 m at the wind farm location. The turbulent boundary layer had a friction velocity of $u_* = 0.2$ m/s, and the aerodynamic roughness length was found to be $z_0 = 0.02$ mm. The parameters u_* and z_0 were determined by fitting a logarithmic velocity profile to the measured averaged velocity.

5. Results

The analysis of the mean streamwise velocity for different wind farm configurations (S_x, S_y) with varying turbine rows, N_r, at different downstream locations, is depicted in Figure 3. The transverse coordinate, y, is made non-dimensional with the farm width, W_F. At a downstream location of $5D$ from the last row of turbines, for all the cases

except $B_{N_r=13}$ and $B_{N_r=15}$, individual wakes of the wind turbines can be observed. The wake deficit at the center of the middle column (c_m, $y/W_F = 0$) of the wind farm is about 40% for all wind farm configurations. A similar wind speed deficit can be observed for the wind turbine column next to the middle column (c_n, $y/W_F = -0.26$). However, the wind speed deficit downstream of the column at the side (c_s, $y/W_F = -0.46$) is lower, 35% for configurations A and B and 30% for configuration C. The reduced wind speed deficit at c_s is due to the horizontal-lateral flow entrainment.

Although at $5D$ downstream at c_m, c_n, and c_s, the velocity deficit is similar for the same configurations with different N_r, at the gap, configurations with the same S_x and S_y with $N_r = 7$ show an increased wind speed deficit compared to those with $N_r > 7$, which exhibit a similar wind speed deficit for the same configurations. In Figure 4, the wake profiles for different wind farm configurations at downstream locations of $5D$, $15D$, and $40D$ with $N_r = 7$ (Figure 4(a), (b), and (c)) and $N_r = 10$ (Figure 4(g), (h), and (i)) are shown. Again, the variation in velocity deficit in the gaps is more evident due to the variation in S_x, S_y, and N_r. At $5D$ downstream with $N_r = 7$, the minimum velocity deficit at the gap is about 25% for configurations A and C and 35% for configuration B. With $N_r = 10$, at this location, the minimum velocity deficit in the gap becomes higher (32% for A, 30% for C, and 38% for B).

At $15D$ downstream, the individual wakes from the turbines are no longer observed. Instead, a wind farm wake can be identified. For the same configurations with varying N_r, the wake profiles exhibit similarities (Figure 3 (b), (e), and (h)). Nevertheless, the influence of S_x and S_y persists at this position for $N_r = 7$ (Figure 4(b)) and $N_r = 10$ (Figure 4(h)). The velocity deficit at c_m is 30%, 32%, and 28% for configurations A, B, and C, respectively. At c_n, it is 28%, 30%, and 25% for configurations A, B, and C. At c_s, it is approximately 20% for all three configurations. At $40D$, for all configurations despite having different N_r, the velocity deficit at c_m, c_n, and c_s is about 20%, 18%, and
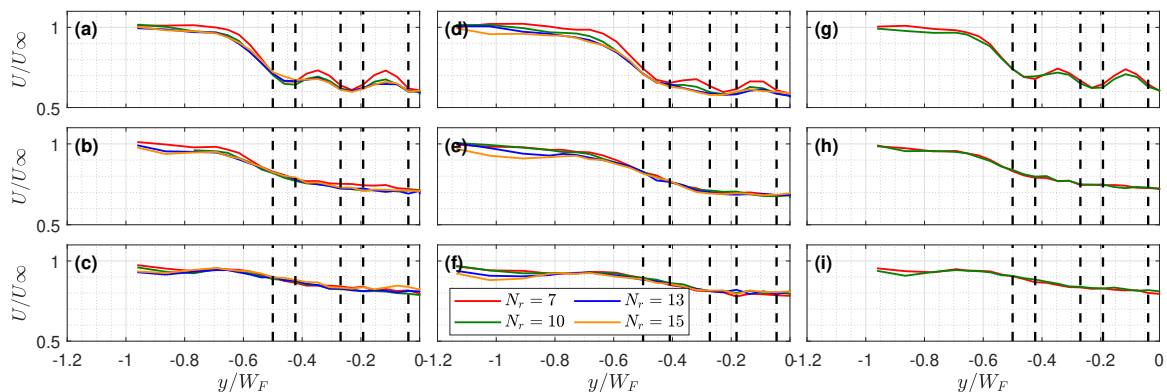

Figure 3. Effect of the number of turbine rows, N_r, on wind farm wake profiles at varying downstream distances and configurations. Rows represent different downstream locations, i.e. $X = 5D$ (a, d, g), $15D$ (b, e, h), and $40D$ (c, f, i), whereas columns represent configurations A, B, and C (left to right). The vertical dashed lines indicate the tips of the porous disk columns.
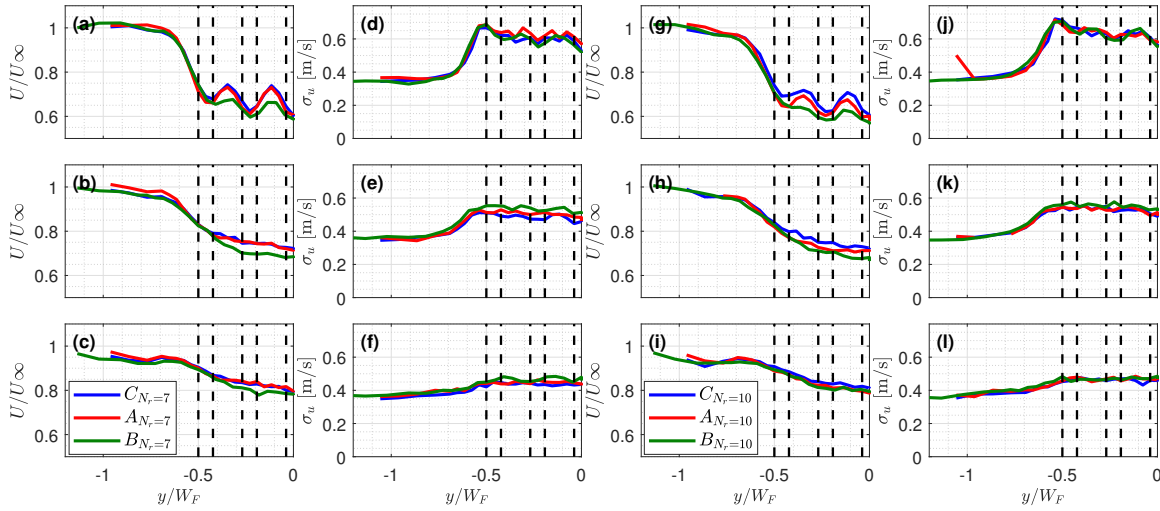
Figure 4. The left two columns show the wake velocity and σ_u profiles for configurations A, B, and C with $N_r = 7$, whereas the right two columns show the same quantities for configurations A, B, and C with $N_r = 10$. Rows show wake velocity and σ_u profiles at $X = 5D, 15D$, and $40D$ (top to bottom) downstream of the farm. The vertical dashed lines indicate the tips of the porous disk columns.
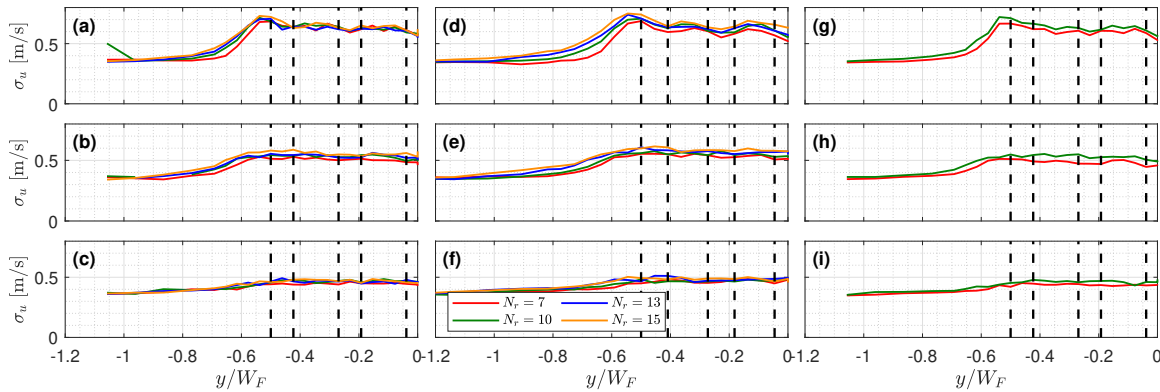
Figure 5. Same as Figure 3, but for σ_u.

10%, respectively.

In Figure 5, similar to the wake profiles, it can be observed that the streamwise standard deviation, σ_u, varies mostly close to the wind farm. At $5D$, where the individual wakes are visible, the σ_u is lower for $N_r = 7$. At the center columns, c_m, σ_u is about 0.5 m/s for $N_r = 7$. It gets higher with N_r for configurations B and C. However, for configuration A, at 5D downstream and at c_m, σ_u remains the same. At this downstream location, σ_u increases gradually toward the side of the farm for all configurations. At c_n and c_s, σ_u increases by 0.05 and 0.1 m/s, respectively, compared to c_m for all cases. At the edge of the farm and $5D$ downstream, the increase is about 0.2 m/s compared to c_m. There is no effect of S_x or S_y observed on σ_u profiles (see Figure 4(d), (e), (f), (j), (k), and (l)).

From the σ_u profiles shown in Figures 4 and 5, it can be observed that close to the farm ($5D$ downstream), the turbulence magnitude is higher at the edge of the farm. This suggests there is more mixing occurring at the edge of the farm just downstream of it, hence more wind speed recovery at the side of the farm, which is also observed in the velocity profiles shown in Figures 3 and 4. However, at $15D$ downstream, this enhanced σ_u at the sides reduces, and σ_u profiles become more homogeneous while the turbulence magnitude no longer depends on N_r. At $40D$ downstream, it dissipates more, and the σ_U becomes more similar to incoming conditions.

From the wake profiles shown in Figure 3 and 4, it can be understood that the effect of S_x, S_y, and N_r is mainly dominant at the near wake. Also, at the near wake, for all configurations when $N_r > 7$, the wake and σ_u profiles show less variation compared to $N_r = 7$. At the far wake, when the individual wakes from the turbines are completely mixed, the wind farm wake becomes similar. The far-wake characteristics of a wind farm, encompassing velocity deficits and turbulence patterns, are significantly influenced by the cumulative thrust coefficient of the entire farm, C_T. This C_T is a function of individual turbine thrust coefficients, C_t, their spatial arrangement (S_x, S_y), and N_r. Notably, we hypothesize the existence of a threshold number of turbine rows, N_r, beyond which further addition of the number of rows and difference in spatial arrangement exhibits a negligible effect on the overall C_T and thus the far-wake behavior. To further investigate this hypothesis, wind farm wakes with different thrust coefficients and reduced N_r need to be studied.

6. Conclusions

In this paper, the cumulative wake generated from a wind farm has been investigated through lidar field measurements performed for the AWAKEN experiment and through wind tunnel tests. The former has provided the opportunity to identify a significant variability in the downstream evolution of wind farm wakes for different incoming wind shear. It has been observed that for lower incoming wind shear, wakes merge, producing a more homogeneous region characterized by a velocity deficit, namely, a wind farm wake. In contrast, for higher wind shear conditions, distinct and well-separated wind turbine wakes are still identified at a downstream distance of $12D$.

Wind tunnel experiments on different wind farm configurations have been conducted at the UTD BLAST wind tunnel. Configurations were modified by adjusting S_x, S_y, and N_r, with wind farms constructed using porous disks to maintain a constant thrust coefficient ($C_t \approx 0.85$). Horizontal profile measurements downstream of the wind farms were obtained through hot-wire anemometry.

The wake deficit close to the wind farm ($5D$ downstream), at the center of the farm wake deficit, is about 40% for all configurations. Horizontal flow entrainment causes less flow deficit at the sides of the wind farm, 35% for configurations A and B and 30% for configuration C. The velocity deficit variation within the gap of the columns is also significant in the near wake for different (S_x, S_y). Also, at this location, for $N_r > 7$, the

wake profiles are almost similar. It is observed that σ_u increases close to the farm with increasing N_r. However, a minimal effect of the farm configuration (S_x, S_y) is observed on the σ_u profiles. Close to the farm, σ_u increases gradually toward the side of it, with the highest being at the edge of the farm, about 40% more compared to the center of the farm. This finding indicates more wind speed recovery at the side of the farm, which can be observed in the velocity profiles as well, where there are higher wind speed at the side of the wind farm compared to the center of the farm. This enhanced σ_u at the edge of the farm reduces downstream and σ_u profiles become more homogeneous.

Acknowledgments

References

[1] Platis A et al 2018 *Scientific Reports* **8** 2163
[2] Platis A et al 2020 *Meteorol. Z.* **29** 355–376.
[3] Schneemann J et al 2020 *Wind Energy Science* **5** 29
[4] Christiansen M B and Hasager C B 2005 *Remote Sensing of Environment* **98** 251
[5] Ahsbahs T, Nygaard N G, Christian Newcombe A and Badger M 2020 *Remote Sensing* **12** 462
[6] Nygaard N G and Christian Newcombe A 2018 *Journal of Physics: Conference Series* **1037** 072008
[7] Puccioni M et al 2023 *Journal of Physics: Conference Series* **2505** 012045
[8] Maas O and Raasch S 2022 *Wind Energy Science* **7(2)** pp.715-739.
[9] Nygaard N G et al 2020 *Journal of Physics: Conference Series* **1618** 062072
[10] Moss C, Maulik R, Moriarty P and Iungo G V 2023. *Wind Energy*
[11] Nygaard N G et al 2016 *Journal of Physics: Conference Series* **Vol. 753, No. 3**, 032020.
[12] Stieren A and Stevens R J 2022 *Flow* **2** p.E21.
[13] Letizia S, Zhan L, and Iungo G V 2021 *Atmos. Meas. Tech.* **14** 2065-2093.
[14] de Jong Helvig S et al 2021 *J. Wind. Eng. Ind. Aerodyn.* **209** p.104485.
[15] Aubrun, S et al 2013 *Journal of Wind Engineering and Industrial Aerodynamics* **120** pp.1-8.
[16] Lignarolo L E M et al 2014 *Journal of Physics: Conference Series* **Vol. 524, No. 1** p. 012163
[17] Lignarolo L E M 2016 *Journal of Renewable and Sustainable Energy* 8(2)
[18] Talluru K M et al 2014 *Measurement Science and Technology* **25(10)** p.105304.
[19] Zhan L et al 2020 *Wind Energy* **23(3)** pp.501-527.